Article:

Zhong, Q-C. and Zeng, Y. (2016) Universal Droop Control of Inverters With Different Types of Output Impedance. IEEE Access, 4. pp. 702-712. ISSN 2169-3536

https://doi.org/10.1109/ACCESS.2016.2526616

Universal Droop Control of Inverters with Different Types of Output Impedance

Qing-Chang Zhong, *Senior Member, IEEE*, and Yu Zeng, *Student Member, IEEE*

***Abstract*—Droop control is a well-known strategy for the parallel operation of inverters. However, the droop control strategy changes its form for inverters with different types of output impedance and, so far, it is impossible to operate inverters with inductive and capacitive output impedances in parallel. In this paper, it is shown that there exists a universal droop control principle for inverters with output impedance having a phase angle between $-\frac{\pi}{2}$ rad and $\frac{\pi}{2}$ rad. It takes the form of the droop control for inverters with resistive output impedance (R-inverters). Hence, the robust droop controller recently proposed in the literature for R-inverters actually provides one way to implement such a universal droop controller that can be applied to all practical inverters without the need of knowing the impedance angle. The small-signal stability of an inverter equipped with the universal droop controller is analyzed and it is shown to be stable when the phase angle of the output impedance changes from $-\frac{\pi}{2}$ rad to $\frac{\pi}{2}$ rad. Both real-time simulation results and experimental results from a test rig consisting of an R-inverter, an L-inverter and a C-inverter operated in parallel are presented to validate the proposed strategy.**

***Index Terms*—C-inverters, L-inverters, output impedance, parallel operation of inverters, R-inverters, robust droop controller, universal droop controller.**

I. Introduction

Power inverters are widely used as the interface to integrate distributed generation (DG) units, renewable energy sources, and energy storage systems [1] into smart grids [2]. They are often operated in parallel for enhanced system redundancy and reliability, as well as for high power and/or low cost. In these applications, the control design for parallel-operated inverters to achieve accurate load sharing among all kinds of sources has become an important issue. To achieve this task, several centralized control techniques with external communication have been reported in the literature [3]. However, the communication link among the inverters generates a technical and economical barrier, especially for remote microgrids [4].

On the contrary, droop control techniques, which make use of the local measurements, are widely used for accurate load sharing without communication [5], [6], [7], [8], [9], [10]. Accurate equal power sharing could be obtained without deviations in either the frequency or the amplitude of the output voltage by adjusting the output impedance and the frequency during the load transients [5]. Another control strategy achieved equal power sharing by drooping the virtual flux instead of the inverter output voltage to avoid the frequency and voltage deviations [6]. For accurate load sharing in proportional to the capacities of the inverters, a small signal injection method was proposed to improve the reactive power sharing accuracy [7], which can also be extended to harmonic current sharing. In [8], a voltage control loop with a direct droop scheme and a power control loop with a complementary inverse droop scheme are implemented for dispatchable sources and nondispatchable ones in a microgrid, respectively.

Inverters equipped with the conventional droop controller are required to have the same per-unit output resistance over a wide range of frequencies. To overcome this limitation, a robust droop controller [9] was proposed to achieve accurate power sharing even when there are numerical errors, disturbances, component mismatches, and parameter drifts. It does no longer require the inverters to have the same per-unit output impedance as long as they are of the same type. However, inverters could have different types of output impedance, which in most of the cases are inductive (L-inverters) around the fundamental frequency but can also be resistive (R-inverters) [5], [9], capacitive (C-inverters) [11], [12], resistive-inductive ($\mathrm{R_L}$-inverters) or resistive-capacitive ($\mathrm{R_C}$-inverters). Figure 1 shows the Bode plots of the output impedance of an L-inverter, an R-inverter, and a C-inverter, from which it can be seen that the impedance of the L-, R-, and C-inverter around the fundamental frequency is mainly inductive, resistive, and capacitive, respectively. Compared with L-inverters, R-inverters can enhance system damping and C-inverters can improve power quality. For inverters with different types of output impedance, droop controllers have different forms [1]. It is still impossible to operate inverters with different types of output impedance in parallel, which is inevitable for large-scale utilization of distributed generations and renewable energy sources.

In the literature, there have been some attempts to find droop controllers that work for more general cases [13], [14], [15], [16], [17], [18]. An orthogonal linear rotational transformation matrix was adopted to modify the real power and the reactive power so that, for L-, R-, and $\mathrm{R_L}$-inverters, the power angle could be controlled by the modified real power and the inverter voltage could be controlled by the modified reactive power [13]. However, the ratio of R/X needs to be known, where R

Some preliminary results were presented at the 39th Annual Conference of the IEEE Industrial Electronics Society (IECON), Vienna, Austria, November 2013.

Q.-C. Zhong is with the Department of Electrical and Computer Engineering, Illinois Institute of Technology, Chicago, IL 60616, USA and also with the Department of Automatic Control and Systems Engineering, The University of Sheffield, Sheffield S1 3JD, United Kingdom. (e-mail: zhongqc@ieee.org)

Y. Zeng is with the Department of Automatic Control and Systems Engineering, The University of Sheffield, Sheffield, S1 3JD, UK.

The financial support from the EPSRC, UK under Grant No. EP/J01558X/1 and EP/J001333/2 is greatly appreciated.

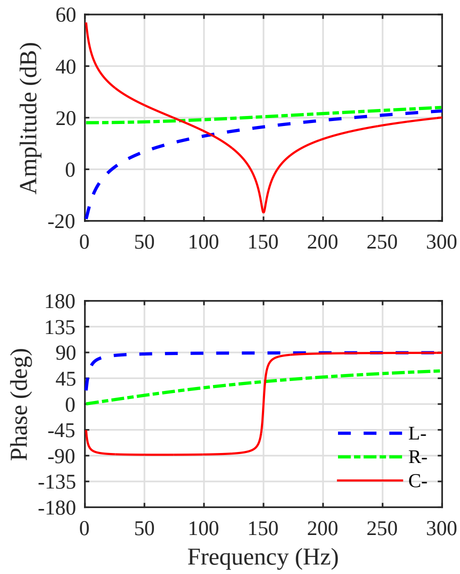

Figure 1. The Bode plots of the output impedance of an L-inverter (with $L = 7$ mH, $R = 0.1\Omega$, and $C_o = 0\,\mu$F), an R-inverter (with $L = 7$ mH, $R = 8\Omega$, and $C_o = 0\,\mu$F), and a C-inverter (with $L = 7$ mH, $R = 0.1\Omega$, and $C_o = 161\,\mu$F).

and X are the resistance and inductance of the inverter output impedance, respectively. A different droop control method added a virtual complex impedance to redesign the angle of the new output impedance to be around $\pi/4$, so that the droop form could be fixed [14]. However, the virtual complex impedance needs to be carefully designed. A generalized droop controller (GDC) based on an adaptive neuro-fuzzy interface system (ANFIS) was developed in [15] to handle a wide range of load change scenarios for L-, R-, and $\mathrm{R_L}$-inverters, but resulted in a complex control structure. Additionally, a real power and reactive power flow controller, which took into account all cases of the R-L relationship, was proposed for three-phase PWM voltage source inverters [16]. But the phase shift needs to be obtained for its power transformation. Moreover, an adaptive droop control method was proposed based on the online evaluation of power decouple matrix [17], which was obtained by the ratio of the variations of the real power and the reactive power under a small perturbation on the voltage magnitude. Recently, an integrated synchronization and control was proposed to operate single-phase inverters in both grid-connected and stand-alone modes [18]. However, all these controllers, called the $\mathrm{R_L}$-controller to facilitate the presentation in the sequel, only work for L-, R-, and $\mathrm{R_L}$-inverters but not for C- or $\mathrm{R_C}$-inverters.

After thoroughly considering this problem, a droop controller for C-, R-, and $\mathrm{R_C}$-inverters, called the $\mathrm{R_C}$-controller, is proposed at first in this paper. Then, the principles of the $\mathrm{R_L}$-controller and the $\mathrm{R_C}$-controller are further explored and clearly illustrated mathematically. Based on these principles, a universal transformation matrix T is identified to develop a universal droop control principle that works for inverters with output impedance having a phase angle between $-\frac{\pi}{2}$ rad and $\frac{\pi}{2}$ rad, which covers any practical L-, R-, C-, $\mathrm{R_L}$-, and $\mathrm{R_C}$-inverters. This universal droop control principle takes the form of the droop control principle for R-inverters, which paves the way for designing universal droop controllers with different methods. In this paper, the robust droop controller proposed in [9] is adopted for implementation. The contribution of this paper lies in revealing this universal droop control principle, mathematically proving it, implementing it with the robust droop controller proposed in [9], and validating it with experiments. Moreover, small-signal stability analysis is carried out for inverters with different types of output impedance [19], [20].

The rest of the paper is organized as follows. In Section II, the conventional droop controller is briefly reviewed with some new insights added. In Section III, after reviewing the droop control strategy that is applicable to L-, R-, and $\mathrm{R_L}$-inverters, a droop control strategy applicable to C-, R-, and $\mathrm{R_C}$-inverters is proposed, together with some further developments for the two strategies. In Section IV, the universal droop control principle is developed and a universal droop controller to implement the principle is proposed, together with small-signal stability analysis. Real-time simulation results are presented in Section V and experimental results obtained from a system consisting of an R-inverter, an L-inverter, and a C-inverter in parallel operation are provided in Section VI for validation, with conclusions made in Section VII.

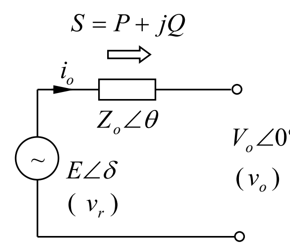

Figure 2. The model of a single-phase inverter.

II. Review of Droop Control for Inverters with the Same Type of Output Impedance

In this section, the widely-adopted droop control strategy is reviewed, with many new insights provided. An inverter can be modeled as a voltage source v_r in series with the output impedance $Z_o\angle\theta$, as shown in Figure 2, where E is the amplitude (or RMS value) of the source voltage and δ, called the power angle, is the phase difference between v_r and v_o. The real power and reactive power delivered from the voltage source v_r to the terminal v_o through the impedance $Z_o\angle\theta$ are

$$P = (\frac{EV_o}{Z_o}\cos\delta - \frac{V_o^2}{Z_o})\cos\theta + \frac{EV_o}{Z_o}\sin\delta\sin\theta, \quad (1)$$

$$Q = (\frac{EV_o}{Z_o}\cos\delta - \frac{V_o^2}{Z_o})\sin\theta - \frac{EV_o}{Z_o}\sin\delta\cos\theta. \quad (2)$$

This characterizes a two-input-two-output control plant from the amplitude E and the phase δ of the source v_r to the real power P and the reactive power Q, as shown in the upper part of Figure 3. The function of a droop control strategy is to generate appropriate amplitude E and phase δ for the

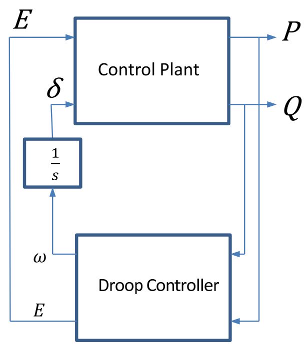

Figure 3. The closed-loop feedback system consisting of the power flow model of an inverter and the droop control strategy.

inverter according to the measured P and Q, that is to close the loop, as shown in Figure 3. This certainly helps understand the essence of droop control and motivates the design of other droop control strategies. Indeed, so far, the majority of the droop controllers are static rather than dynamic [21] and other dynamic droop controllers should/could be developed to improve the performance. Anyway, this is not the main concern of this paper and will not be discussed further.

In practice, it is often assumed that δ is small. In this case,

$$P \approx (\frac{EV_o}{Z_o} - \frac{V_o^2}{Z_o})\cos\theta + \frac{EV_o}{Z_o}\delta\sin\theta, \tag{3}$$

$$Q \approx (\frac{EV_o}{Z_o} - \frac{V_o^2}{Z_o})\sin\theta - \frac{EV_o}{Z_o}\delta\cos\theta. \tag{4}$$

This leads to decoupled relationships between the inputs and the outputs, which change with the impedance angle θ. For example, when the output impedance is inductive ($\theta = \frac{\pi}{2}$ rad), P is roughly proportional to δ, noted as $P \sim \delta$, and Q is roughly proportional to E, noted as $Q \sim E$. According to this, the well-known droop control strategy, that is to droop the frequency when the real power increases and to droop the voltage when the reactive power increases, can be adopted. The cases when the output impedance is resistive ($\theta = 0$ rad) and capacitive ($\theta = -\frac{\pi}{2}$ rad) can be analyzed similarly, which results in different droop control strategies [1]. The cases when the impedance is inductive (L-inverter), capacitive (C-inverter), resistive (R-inverter), resistive-capacitive ($\mathrm{R_C}$-inverter), and resistive-inductive ($\mathrm{R_L}$-inverter) are summarized in Table I for convenience. Apparently, the input-output relationships are different and so are the droop controllers. This holds true for the conventional droop controller as well as the robust droop controller [9], which is robust against variations of output impedance, component mismatches, parameter drifts, and disturbances etc.

Since the droop control strategies change the form when the output impedance θ changes, it is difficult to operate inverters with different types of output impedance in parallel. In particular, the droop control strategies for L-inverters and C-inverters act in the opposite way and the parallel operation of a C-inverter with an L-inverter certainly does not work if these droop control strategies are employed.

Table I

DROOP CONTROLLERS FOR L-, R-, C-, $\mathrm{R_L}$-, AND $\mathrm{R_C}$-INVERTERS.

Inverter type	θ	Input-output/Droop relationship	Droop controller
L-	$\frac{\pi}{2}$	$P \sim \delta$	$E = E^* - nQ$
		$Q \sim E$	$\omega = \omega^* - mP$
R-	$0°$	$P \sim E$	$E = E^* - nP$
		$Q \sim -\delta$	$\omega = \omega^* + mQ$
C-	$-\frac{\pi}{2}$	$P \sim -\delta$	$E = E^* + nQ$
		$Q \sim -E$	$\omega = \omega^* + mP$
$\mathrm{R_C}$-	$(-\frac{\pi}{2}, 0)$	Coupled	Depends on θ
$\mathrm{R_L}$-	$(0, \frac{\pi}{2})$	Coupled	Depends on θ

III. DROOP CONTROL FOR INVERTERS WITH DIFFERENT TYPES OF OUTPUT IMPEDANCE

A. *Parallel Operation of L-, R-, and* $\mathrm{R_L}$*-inverters*

Some works [13], [14], [15] have been reported in the literature to investigate the parallel operation of inverters with different types of output impedance, although they are limited to the parallel operation of L-, R-, and $\mathrm{R_L}$-inverters. This involves the introduction of the orthogonal transformation matrix

$$T_L = \begin{bmatrix} \sin\theta & -\cos\theta \\ \cos\theta & \sin\theta \end{bmatrix} \tag{5}$$

to convert the real power and the reactive power when $\theta \in (0, \frac{\pi}{2}]$ into

$$\begin{bmatrix} P_L \\ Q_L \end{bmatrix} = T_L \begin{bmatrix} P \\ Q \end{bmatrix} = \begin{bmatrix} \frac{EV_o}{Z_o}\sin\delta \\ \frac{EV_o}{Z_o}\cos\delta - \frac{V_o^2}{Z_o} \end{bmatrix}. \tag{6}$$

If δ is assumed small, roughly

$$P_L \sim \delta \quad \text{and} \quad Q_L \sim E, \tag{7}$$

which results in the droop controller of the form

$$E = E^* - nQ_L \tag{8}$$

$$\omega = \omega^* - mP_L. \tag{9}$$

This is called the $\mathrm{R_L}$-controller in order to facilitate the presentation in the sequel. Here, n and m are called the droop coefficients. This controller has the same form as the droop controller for L-inverters but the impedance angle θ needs to be known in order to obtain the transformed power P_L and Q_L from (6); see [13], [14], [15].

B. *Parallel Operation of* $\mathrm{R_C}$*-, R-, and C-inverters*

Following the same line of thinking, the transformation matrix

$$T_C = \begin{bmatrix} -\sin\theta & \cos\theta \\ -\cos\theta & -\sin\theta \end{bmatrix} \tag{10}$$

can be introduced for C-, R- or $\mathrm{R_C}$-inverters with $\theta \in [-\frac{\pi}{2}, 0)$ to convert the real power and the reactive power into

$$\begin{bmatrix} P_C \\ Q_C \end{bmatrix} = T_C \begin{bmatrix} P \\ Q \end{bmatrix} = \begin{bmatrix} -\frac{EV_o}{Z_o}\sin\delta \\ -\frac{EV_o}{Z_o}\cos\delta + \frac{V_o^2}{Z_o} \end{bmatrix}. \quad (11)$$

In this case, for a small δ, roughly

$$P_C \sim -\delta \quad \text{and} \quad Q_C \sim -E, \quad (12)$$

which results in the droop controller of the form

$$E = E^* + nQ_C \quad (13)$$
$$\omega = \omega^* + mP_C. \quad (14)$$

This is called the $\mathrm{R_C}$-controller in order to facilitate the presentation in the sequel and it has the same form as the droop controller for C-inverters, which was proposed in [11], [12]. Again, the impedance angle θ needs to be known in order to obtain the transformed active power P_C and reactive power Q_C from (11). Apparently, this controller does not work for L- or $\mathrm{R_L}$-inverters because of the negative signs in (8-9).

C. Further Development of the $\mathrm{R_L}$*-controller and the* $\mathrm{R_C}$*-controller*

The eigenvalues of T_L in (5) are $\sin\theta \pm j\cos\theta$, of which the real part $\sin\theta$ is positive for impedance with $\theta \in (0, \frac{\pi}{2}]$. According to the properties of the linear transformation [22] and the mapping described by (6), it can be seen that P and Q have positive correlations with P_L and Q_L, respectively. This can be described as

$$P \sim P_L \quad \text{and} \quad Q \sim Q_L. \quad (15)$$

So the relationship shown in (7) can be passed onto P and Q as

$$P \sim P_L \sim \delta \quad \text{and} \quad Q \sim Q_L \sim E. \quad (16)$$

In other words, for output impedance with $\theta \in (0, \frac{\pi}{2}]$, the real power P always has positive correlation with the power angle δ and the reactive power Q always has positive correlation with the voltage E. Hence, the $\mathrm{R_L}$-controller can also be designed as

$$E = E^* - nQ, \quad (17)$$
$$\omega = \omega^* - mP, \quad (18)$$

which is directly related to the real power P and the reactive power Q, regardless of the impedance angle θ. In other words, the effect of the impedance angle θ has been removed as long as it satisfies $\theta \in (0, \frac{\pi}{2}]$.

In order to better understand the transformation matrix (5), the transformation (6) can actually be rewritten as

$$\begin{aligned} P_L + jQ_L &= P\sin\theta - Q\cos\theta + j(P\cos\theta + Q\sin\theta) \\ &= e^{j(\frac{\pi}{2}-\theta)}(P + jQ), \end{aligned}$$

where $j = \sqrt{-1}$. In other words, the transformation (5) rotates the power vector $P + jQ$ by $\frac{\pi}{2} - \theta$ rad onto the axis aligned with the $L-$inverter, as shown in Figure 4(a), so that the droop controller (17-18) can be formed.

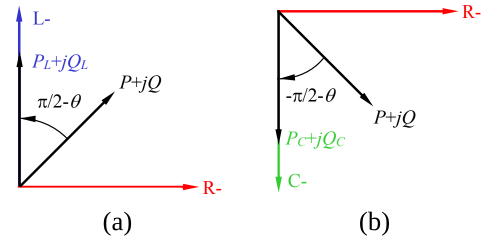

Figure 4. Interpretation of the transformation matrices: (a) T_L and (b) T_C (b) .

Similarly, for the $\mathrm{R_C}$-controller, the eigenvalues of T_C in (10) are $-\sin\theta \pm j\cos\theta$, of which the real part $-\sin\theta$ is positive for any output impedance with $\theta \in [-\frac{\pi}{2}, 0)$. Hence, according to the mapping described by (11), P and Q have positive correlations with P_C and Q_C, respectively. This can be described as

$$P \sim P_C \quad \text{and} \quad Q \sim Q_C. \quad (19)$$

So the relationship shown in (12) can be passed onto P and Q as

$$P \sim P_C \sim -\delta \quad \text{and} \quad Q \sim Q_C \sim -E. \quad (20)$$

In other words, for impedance with $\theta \in [-\frac{\pi}{2}, 0)$, the real power P always has negative correlation with the power angle δ and the reactive power Q always has negative correlation with the voltage E. Then, the $\mathrm{R_C}$-controller can also be designed as

$$E = E^* + nQ, \quad (21)$$
$$\omega = \omega^* + mP, \quad (22)$$

which is also directly related to the real power P and the reactive power Q. The effect of the impedance angle θ has been removed as long as it satisfies $\theta \in [-\frac{\pi}{2}, 0)$.

Also similarly, to better understand the transformation matrix (10), the transformation (11) can be rewritten as

$$\begin{aligned} P_C + jQ_C &= -P\sin\theta + Q\cos\theta + j(-P\cos\theta - Q\sin\theta) \\ &= e^{j(-\frac{\pi}{2}-\theta)}(P + jQ). \end{aligned}$$

In other words, the transformation (10) actually rotates the power vector $P + jQ$ by $-\frac{\pi}{2} - \theta$ rad onto the axis aligned with the $C-$inverter, as shown in Figure 4(b), to form the droop controller (21-22).

In summary, the $\mathrm{R_L}$-controller (17-18) can be applied to inverters with the output impedance satisfying $\theta \in (0, \frac{\pi}{2}]$ and the $\mathrm{R_C}$-controller can be applied to inverters with the output impedance satisfying $\theta \in [-\frac{\pi}{2}, 0)$. This widens the application range of the L-controller and the C-controller. However, the $\mathrm{R_L}$-controller cannot be applied to C- or $\mathrm{R_C}$-inverters, and the $\mathrm{R_C}$-controller cannot be applied to L- or $\mathrm{R_L}$-inverters, either. There is still a need to develop a controller that is applicable to L-, R-, C-, $\mathrm{R_L}$-, and $\mathrm{R_C}$-inverters.

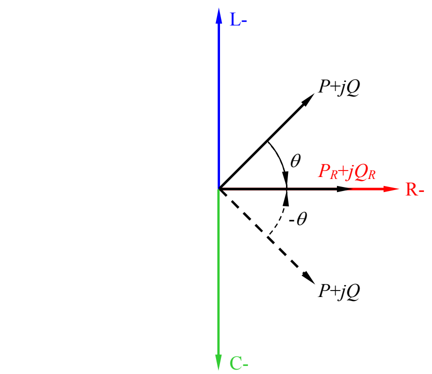

Figure 5. Interpretation of the universal transformation matrix T.

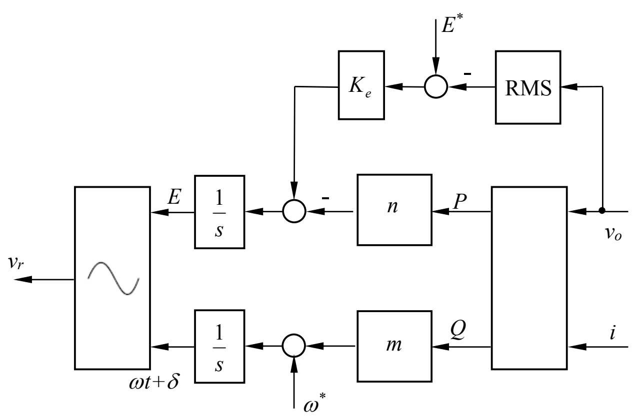

Figure 6. One implementation of the universal droop controller, which takes the form of the robust droop controller for R-inverters proposed in [9], [1].

IV. Universal Droop Controller

A. Basic Principle

Following the above analysis, consider the transformation matrix

$$T = \begin{bmatrix} \cos\theta & \sin\theta \\ -\sin\theta & \cos\theta \end{bmatrix}. \tag{23}$$

It transforms the real power P and the reactive power Q to

$$\begin{bmatrix} P_R \\ Q_R \end{bmatrix} = T \begin{bmatrix} P \\ Q \end{bmatrix} = \begin{bmatrix} \frac{EV_o}{Z_o}\cos\delta - \frac{V_o^2}{Z_o} \\ -\frac{EV_o}{Z_o}\sin\delta \end{bmatrix}, \tag{24}$$

which can be rewritten as

$$\begin{aligned} P_R + jQ_R &= P\cos\theta + Q\sin\theta + j(-P\sin\theta + Q\cos\theta) \\ &= e^{-j\theta}(P + jQ). \end{aligned}$$

As shown in Figure 5, this transformation rotates the power vector $P+jQ$ by $-\theta$ onto the axis aligned with the R-inverter, i.e., clockwise when $\theta \in [0, \frac{\pi}{2})$ and counter-clockwise when $\theta \in (-\frac{\pi}{2}, 0]$. Indeed, the eigenvalues of T in (23) are $\cos\theta \pm j\sin\theta$, of which the real part $\cos\theta$ is positive for any output impedance with $\theta \in (-\frac{\pi}{2}, \frac{\pi}{2})$. According to the properties of the linear transformation [22] and the mapping described by (24), P and Q are proven to have positive correlations with P_R and Q_R, respectively. This can be described as

$$P \sim P_R \quad \text{and} \quad Q \sim Q_R. \tag{25}$$

According to (24), for a small δ, there are

$$P_R \sim E \quad \text{and} \quad Q_R \sim -\delta. \tag{26}$$

Combining these two, there is

$$P \sim P_R \sim E \quad \text{and} \quad Q \sim Q_R \sim -\delta \tag{27}$$

for any $\theta \in (-\frac{\pi}{2}, \frac{\pi}{2})$. This basically indicates that the real power P always has positive correlation with the voltage E and the reactive power Q always has negative correlation with the power angle δ for any impedance angle $\theta \in (-\frac{\pi}{2}, \frac{\pi}{2})$. This results in the following conventional universal droop controller

$$E = E^* - nP, \tag{28}$$
$$\omega = \omega^* + mQ, \tag{29}$$

which is applicable to inverters with output impedance satisfying $\theta \in (-\frac{\pi}{2}, \frac{\pi}{2})$. Note that this droop controller (28-29) takes the form of the droop controller for R-inverters. The main contribution of this paper is to have revealed this fact and formally proven it.

Theoretically, when the impedance is purely inductive ($\theta = \frac{\pi}{2}$ rad) or capacitive ($\theta = -\frac{\pi}{2}$ rad), this relationship does not hold but, in practice, there is always an equivalent series resistance (ESR) in series with the filter inductor so the controller (28-29) is actually applicable to all practical L-, R-, C-, $\mathrm{R_L}$-, and $\mathrm{R_C}$-inverters.

B. Implementation

There are many ways to implement the universal droop control principle revealed in the previous subsection. The most natural way is to take the robust droop controller proposed in [9], [1], which is re-drawn as shown in Figure 6 for the convenience of the reader. This controller can be described as:

$$\dot{E} = K_e(E^* - V_o) - nP, \tag{30}$$
$$\omega = \omega^* + mQ, \tag{31}$$

In the steady state, there is

$$nP = K_e(E^* - V_o), \tag{32}$$

which means the output voltage

$$V_o = E^* - \frac{nP}{K_e E^*}E^*. \tag{33}$$

Here, $\frac{nP}{K_e E^*}$ is the voltage drop ratio, which can be maintained within the desired range via choosing a large K_e. Moreover, as long as K_e is chosen the same for all inverters operated in parallel, the right-hand side of (32) will be the same, which guarantees accurate real power sharing. For more details, see [9]. Although this controller is known, the contribution of this paper is to reveal that this controller is actually universal for all practical L-, R-, C-, $\mathrm{R_L}$-, and $\mathrm{R_C}$-inverters to achieve parallel operation.

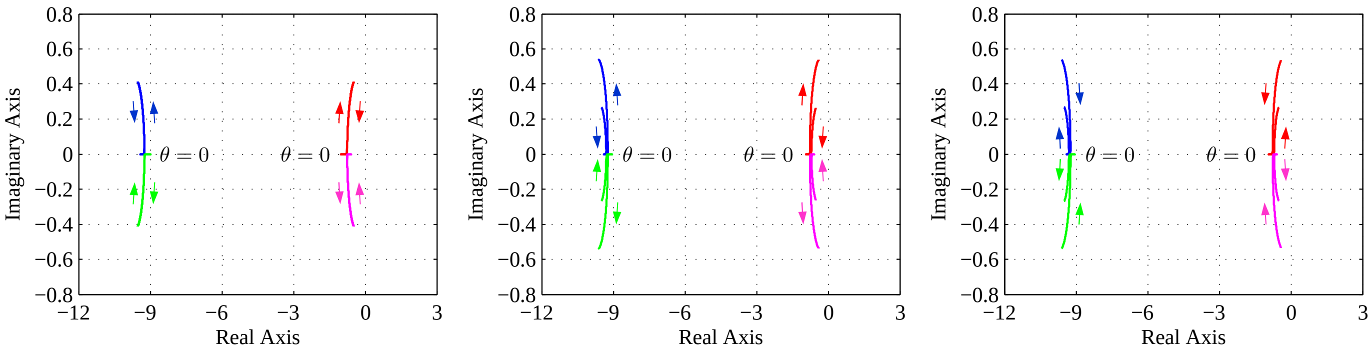

(a) (b) (c)

Figure 7. The root loci of the small-signal model of the closed-loop system (43) when θ changes from $-\frac{\pi}{2}$ to $\frac{\pi}{2}$: (a) with a resistive load $R = 8\Omega$, (b) with a resistive-inductive load $7.6 + 2.76j$, (c) with a resistive-capacitive load $7.6 - 2.76j$.

C. Small-signal Stability

It is a great challenge to analyze the stability of inverters in parallel operation. Here, the small-signal stability of one inverter equipped with the universal droop controller (30-31) is analyzed.

Considering small disturbances around the stable equilibrium operation point (δ_e, V_{oe}, E_e), where E_e is the magnitude of the inverter source voltage, V_{oe} is the magnitude of the load voltage and δ_e is the phase angle difference between the inverter source voltage and the load voltage. Linearizing (1) and (2) around the equilibrium leads to

$$\Delta P(s) = \frac{V_{oe}(\cos\delta_e\cos\theta + \sin\delta_e\sin\theta)}{Z_o}\Delta E(s) + \frac{E_e V_{oe}(-\sin\delta_e\cos\theta + \cos\delta_e\sin\theta)}{Z_o}\Delta\delta(s), \quad (34)$$

$$\Delta Q(s) = \frac{V_{oe}(\cos\delta_e\sin\theta - \sin\delta_e\cos\theta)}{Z_o}\Delta E(s) - \frac{E_e V_{oe}(\sin\delta_e\sin\theta + \cos\delta_e\cos\theta)}{Z_o}\Delta\delta(s). \quad (35)$$

Similarly, the universal droop controller (30-31) can be linearized around the equilibrium as

$$s\Delta E(s) = -n\Delta P(s), \quad (36)$$

$$\Delta\omega(s) = m\Delta Q(s). \quad (37)$$

Additionally, there is

$$\Delta\omega(s) = s\Delta\delta(s). \quad (38)$$

Note that the real power and the reactive power are normally measured using a low pass filter $\frac{\omega_f}{s+\omega_f}$. Combining the above equations, the small-signal model of the closed-loop system is

$$s\Delta E(s) = -n\cdot\frac{\omega_f}{s+\omega_f}\cdot[\frac{V_{oe}(\cos\delta_e\cos\theta + \sin\delta_e\sin\theta)}{Z_o}\Delta E(s) + \frac{E_e V_{oe}(-\sin\delta_e\cos\theta + \cos\delta_e\sin\theta)}{Z_o}\Delta\delta(s)], \quad (39)$$

$$s\Delta\delta(s) = m\cdot\frac{\omega_f}{s+\omega_f}\cdot[\frac{V_{oe}(\cos\delta_e\sin\theta - \sin\delta_e\cos\theta)}{Z_o}\Delta E(s) - \frac{E_e V_{oe}(\sin\delta_e\sin\theta + \cos\delta_e\cos\theta)}{Z_o}\Delta\delta(s)], \quad (40)$$

which leads to the following fourth-order homogeneous equation

$$as^4\Delta\delta(s) + bs^3\Delta\delta(s) + cs^2\Delta\delta(s) + ds\Delta\delta(s) + e\Delta\delta(s) = 0, \quad (41)$$

with

$$a = Z_o^2$$
$$b = 2Z_o^2\omega_f$$
$$c = Z_o\omega_f(V_{oe}(\cos\delta_e\cos\theta+\sin\delta_e\sin\theta)(n+mE_e)+Z_o\omega_f) \quad (42)$$
$$d = Z_o\omega_f^2 V_{oe}(\cos\delta_e\cos\theta + \sin\delta_e\sin\theta)(n + mE_e)$$
$$e = mnE_e\omega_f^2 V_{oe}^2.$$

The system stability can be analyzed by investigating the characteristic equation

$$as^4 + bs^3 + cs^2 + ds + e = 0. \quad (43)$$

For the experimental system to be described later in Section VI, the root-locus plots of this characteristic equation when θ changes from $-\frac{\pi}{2}$ rad to $\frac{\pi}{2}$ rad are shown in Figure 7 with

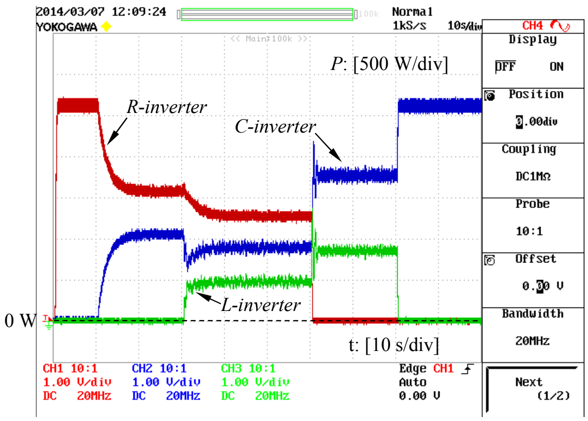

(a) Real power

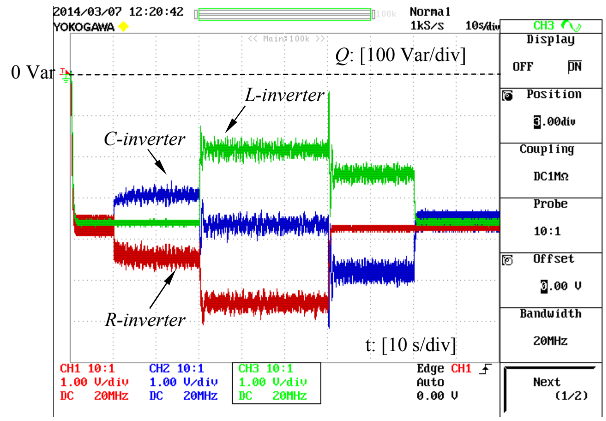

(b) Reactive power

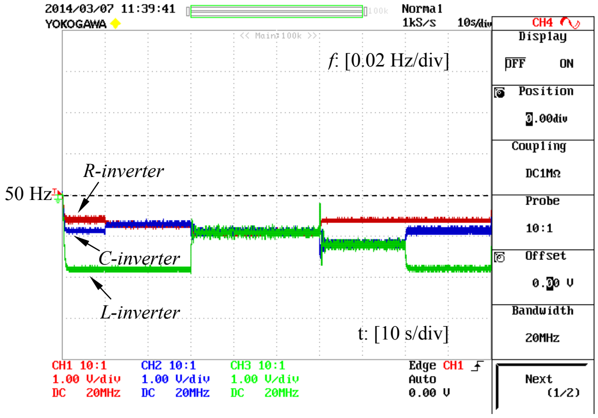

(c) Frequencies

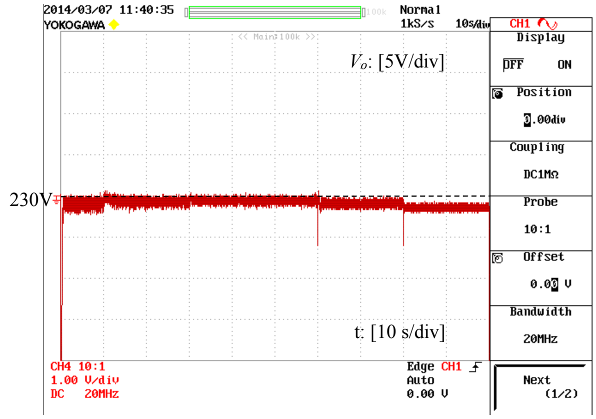

(d) RMS output voltage

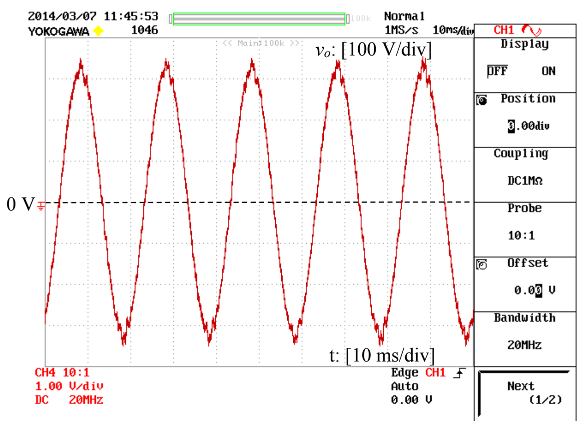

(e) Output voltage

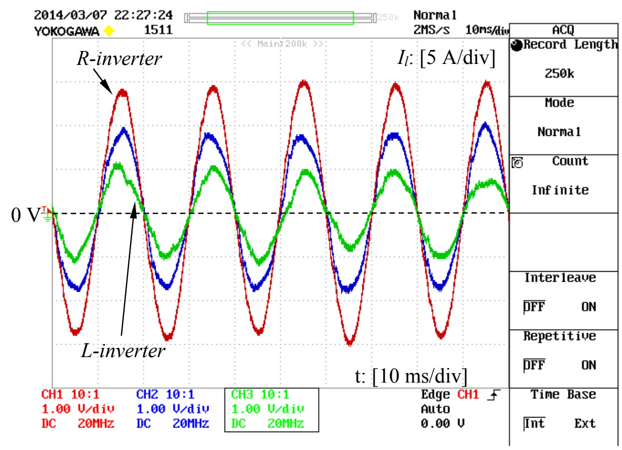

(f) Inductor currents

Figure 8. Real-time simulation results of three inverters with different types of output impedance operated in parallel.

droop coefficients $n = 0.48$ and $m = 0.03$ for three cases of different loads, i.e, a resistive load $R = 8\Omega$, a resistive-inductive load $7.6+2.76j$, and a resistive-capacitive load $7.6-2.76j$. It can be seen that the system is stable for all three cases. Note that, according to (33), V_{oe} is independent from the output impedance angle θ. Thus, as long as the load is not changed, it remains as a constant at the equilibrium when the inverter output impedance angle θ changes. E_e changes with the impedance angle θ but can be calculated according to V_{oe} and the given load.

V. Real-time simulation results

In order to validate the proposed universal droop control principle, real-time simulations were carried out on an OPAL RT real-time digital simulator. Three single-phase inverters powered by three separate 400 V DC voltage supplies were operated together to power a $20\,\Omega$ linear load. The capacities of Inverters 1 (L-inverter), 2 (C-inverter) and 3 (R-inverter with a virtual 4Ω resistor) were 1 KVA, 2 KVA and 3KVA, respectively. It is expected that $P_2 = 2P_1$, $Q_2 = 2Q_1$, $P_3 = 3P_1$ and $Q_3 = 3Q_1$. The PWM switching frequency was 10 kHz and the line frequency of the system was 50 Hz. The rated output voltage was 230 V and $K_e = 10$. The filter inductor was $L = 0.55$ mH with a parasitic resistance of $0.3\,\Omega$ and the filter capacitor C was $20\,\mu$F. According to [23], the desired voltage drop ratio $\frac{n_i S_i^*}{K_e E^*}$ was chosen as 0.25% and the frequency boost ratio $\frac{m_i S_i^*}{\omega^*}$ was 0.1% so the droop coefficients are $n_1 = 0.0057$, $n_2 = 0.0029$, $n_3 = 0.0019$, $m_1 = 3.1416 \times 10^{-4}$, $m_2 = 1.5708 \times 10^{-4}$ and $m_3 = 1.0472 \times 10^{-4}$.

The real-time simulation results are shown in Figure 8. At $t = 0s$, the three inverters were operated separately with the load connected to the R-inverter only. Then, at $t = 10s$, the C-inverter was connected in parallel with the R-inverter and the two inverters shared the real power and reactive power accurately in the ratio of 2:3. At $t = 30s$, the L-inverter was put into parallel operation. The three inverters shared the real power and reactive power accurately in the ratio of 1:2:3. Then the R-inverter was disconnected at $t = 60s$ and the C-inverter and the L-inverter shared the power accurately in the ratio of 2:1. Finally, the L-inverter was disconnected at t=80s and the load was powered by the C-inverter only. The frequency and the voltage were regulated to be very close to the rated values, respectively, as can be seen from Figure 8(c) and (d).

The waveforms of the load voltage and the inductor currents of the three inverters after taking away the switching ripples with a hold filter when the three inverters were in parallel operation are shown in Figure 8(e) and (f). It can be seen that indeed the three inverters shared the load accurately in the ratio of 1:2:3.

VI. Experimental Validation

To further validate the proposed universal droop controller, experiments were carried out on a system consisting of three inverters operated in parallel, as shown in Figure 9. Each single-phase inverter is powered by a 30 V DC voltage supply and loaded with a $3.8\,\Omega$ resistor in series with two 2.2 mH

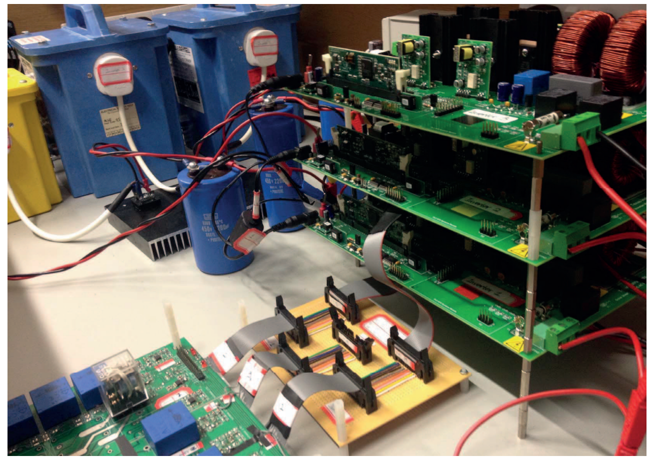

Figure 9. The experimental set up consisting of an L-inverter, an R-inverter, and a C-inverter in parallel operation.

inductors. Since the aim of this paper is to address the parallel operation of inverters with different types of output impedance, the case with a nonlinear load is not considered. The filter inductor is $L = 7$ mH with a parasitic resistance of $1\,\Omega$ and the filter capacitor is $C = 1\,\mu$F, which is not optimized. The PWM switching frequency is 10 kHz; the rated system frequency is 50 Hz and the cut-off frequency ω_f of the measuring filter is 10 rad/s. The rated output voltage is 12 V and $K_e = 20$. The desired voltage drop ratio $\frac{n_i S_i^*}{K_e E^*}$ is chosen as 10% and the frequency boost ratio $\frac{m_i S_i^*}{\omega^*}$ is chosen as 0.5%. Here the subscript i is the inverter index. These inverters are operated as an R-inverter with a virtual 8 Ω resistor [5], [9], a C-inverter with a virtual 161 μF capacitor in series with a virtual 2.5 Ω resistor [11], [12], and an original L-inverter, respectively.

A. Case I: Parallel Operation of an L-inverter and a C-inverter

In this case, the L-inverter and the C-inverter were designed to have the power ratio of 1:2, with $P_2 = 2P_1$ and $Q_2 = 2Q_1$. The droop coefficients are $n_1 = 0.96$, $n_2 = 0.48$, $m_1 = 0.06$ and $m_2 = 0.03$. The experimental results are shown in Figure 10. At $t = 3$ s, the C-inverter was started to take the load. Then, at about $t = 6$ s, the L-inverter was started to synchronize with the C-inverter. At about $t = 12$ s, the L-inverter was paralleled with the C-inverter. They shared the power with a ratio of 1:2. The inverter output voltage and inductor currents were regulated well and the currents were shared accurately with a ratio of 1:2. Note that the spikes in the frequency before the connection were caused by the phase resetting (zero crossing) applied for synchronization.

B. Case II: Parallel Operation of an L-inverter, a C-inverter, and an R-inverter

In this case, the L-inverter, the C-inverter, and the R-inverter were designed to have a power capacity ratio of 1:2:3, with $P_3 = 1.5P_2 = 3P_1$ and $Q_3 = 1.5Q_2 = 3Q_1$. The droop coefficients are $n_1 = 1.44$, $n_2 = 0.72$, $n_3 = 0.48$, $m_1 = 0.09$, $m_2 = 0.045$, and $m_3 = 0.03$. The parallel operation of the

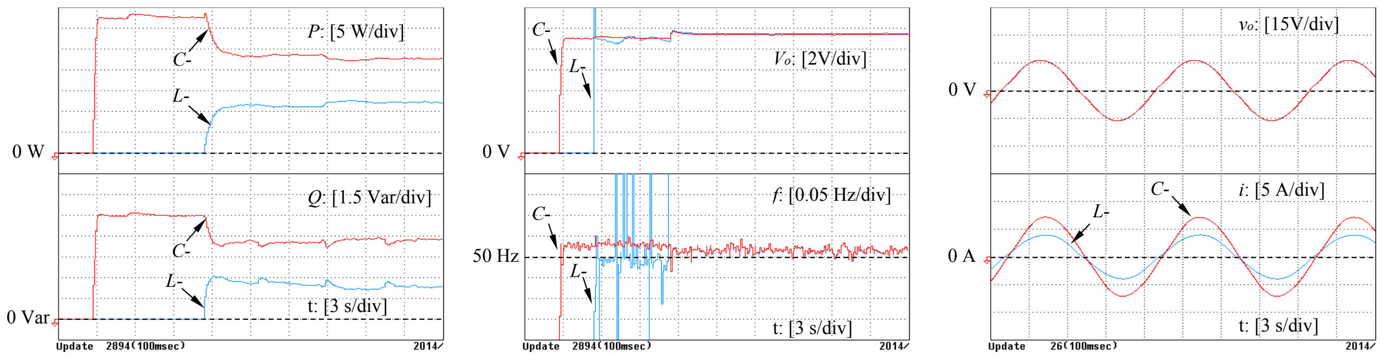

(a) (b) (c)

Figure 10. Parallel operation of an L-inverter and a C-inverter: (a) P and Q, (b) V_o and f, (c) load voltage v_o and i.

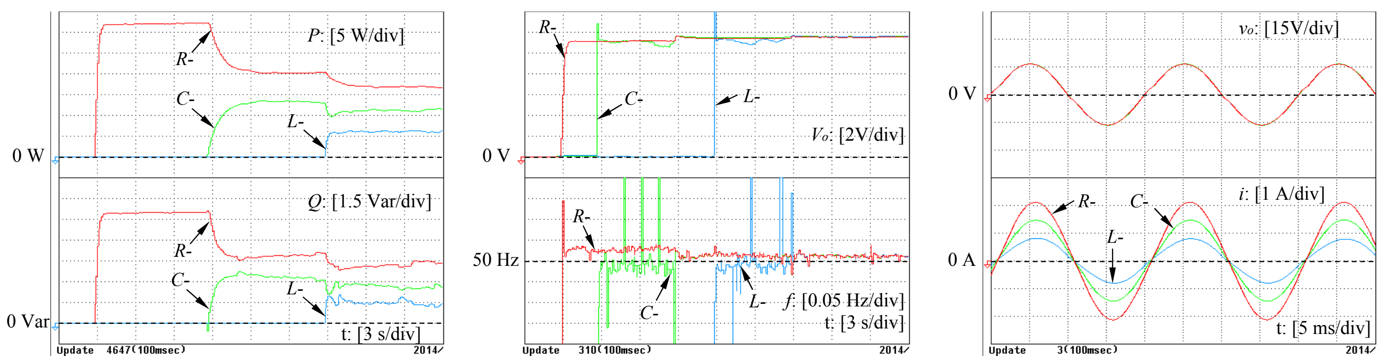

(a) (b) (c)

Figure 11. Parallel operation of an L-inverter, a C-inverter, and an R-inverter: (a) P and Q, (b) V_o and f, (c) v_o and i.

Table II
STEADY-STATE PERFORMANCE OF THREE INVERTERS IN PARALLEL OPERATION

Variable	R-&L-&C-inverters
Apparent power 1	6.07+1.54j VA
Apparent power 2	11.62+2.83j VA
Apparent power 3	16.60+3.97j VA
Output voltage	11.55 V(rms)
Inductor current 1	0.54 A(rms)
Inductor current 2	1.03 A(rms)
Inductor current 3	1.48 A(rms)
Frequency f	50.016 Hz
Current sharing error $\frac{I_3-3I_1}{4I_3}\times 100\%$	-2.4%
Voltage drop $\frac{E^*-V_o}{E^*}\times 100\%$	3.8%
Frequency drop $\frac{f^*-f}{f^*}\times 100\%$	0.03%

three inverters is tested, and the experimental results are shown in Figure 11.

At $t = 3$s, the R-inverter was started to supply the load. Then, at about $t = 6$ s, the C-inverter was started and began to synchronize with the R-inverter. As shown in Figure 11(b), the RMS output voltage of the C-inverter stepped up to be almost the same as that of the R-inverter and the frequency of the C-inverter stepped up to be around 50Hz. At about $t = 12$ s, the C-inverter was connected to the load and thus in parallel with the R-inverter. As shown in Figure 11(a), after a short transient, the R-inverter and the C-inverter shared the real power and the reactive power with the ratio of 3:2, as designed. As shown in Figure 11(b), the RMS value of the output voltage and the frequency of both inverters became the same. The inverter output voltage RMS value slightly increased and the R-inverter frequency decreased a little bit. Then, at about $t = 15$ s, the L-inverter was started to synchronize with the terminal voltage established by the R-inverter and the C-inverter. As shown in Figure 11(b), the RMS output voltage of the L-inverter stepped up to be almost the same as that of the load and the frequency of the L-inverter stepped up to be around 50Hz. After that, at about $t = 21$ s, the L-inverter was connected to the load and thus in parallel with the R-inverter and the C-inverter. As shown in Figure 11(a), the L-inverter, the C-inverter, and the R-inverter shared the real power and the reactive power with the designed ratio of 1:2:3, as designed. As shown in Figure 11(b), the RMS value of the output voltage and the frequency of these three inverters became the same. The RMS voltage of the load slightly increased and the frequency decreased a little bit. The load voltage was regulated well and the inverter currents were shared accurately with the ratio of 1:2:3 in the steady state, as shown in Figure 11(c).

The measured steady-state performance is summarized and shown in Table II. The current sharing error is just -2.4%, which is very low taking into account that the inverters were not optimized. The performance for voltage regulation and frequency regulation is very good too.

VII. Conclusions

In this paper, a universal droop control principle has been proposed for inverters with output impedance having an impedance angle between $-\frac{\pi}{2}$ rad and $\frac{\pi}{2}$ rad to achieve parallel operation. Coincidentally, the robust droop controller recently proposed in the literature for inverters with resistive output impedance (R-inverters) actually offers one way to implement this principle. In other words, it can be applied to any practical inverters having an impedance angle between $-\frac{\pi}{2}$ rad and $\frac{\pi}{2}$ rad. Small-signal stability analysis carried out for an inverter equipped with the universal droop controller when the impedance angle changes from $-\frac{\pi}{2}$ rad to $\frac{\pi}{2}$ rad for different loads shows that the system is stable. Moreover, experimental results have demonstrated the effectiveness of the universal droop controller for the parallel operation of inverters with different types of output impedance, achieving accurate proportional power sharing, tight voltage regulation and very tight frequency regulation.

References

[1] Q.-C. Zhong and T. Hornik, *Control of Power Inverters in Renewable Energy and Smart Grid Integration*. Wiley-IEEE Press, 2013.

[2] X. Fang, S. Misra, G. Xue, and D. Yang, "Smart grid - the new and improved power grid: A survey," *IEEE Commun. Surveys Tuts.*, vol. 14, no. 4, pp. 944–980, 2012.

[3] H. Mahmood, D. Michaelson, and J. Jiang, "Accurate reactive power sharing in an islanded microgrid using adaptive virtual impedances," *IEEE Trans. Power Electron.*, vol. 30, no. 3, pp. 1605–1617, Mar. 2015.

[4] I. Nutkani, P. C. Loh, and F. Blaabjerg, "Droop scheme with consideration of operating costs," *IEEE Trans. Power Electron.*, vol. 29, no. 3, pp. 1047–1052, 2014.

[5] J. M. Guerrero, L. G. de Vicuna, J. Matas, M. Castilla, and J. Miret, "Output impedance design of parallel-connected UPS inverters with wireless load-sharing control," *IEEE Trans. Ind. Electron.*, vol. 52, no. 4, pp. 1126–1135, May. 2005.

[6] J. Hu, J. Zhu, D. Dorrell, and J. Guerrero, "Virtual flux droop method - a new control strategy of inverters in microgrids," *IEEE Trans. Ind. Electron.*, vol. 29, no. 9, pp. 4704–4711, Sept. 2014.

[7] A. Tuladhar, H. Jin, T. Unger, and K. Mauch, "Control of parallel inverters in distributed AC power systems with consideration of line impedance effect," *IEEE Trans. Ind. Appl.*, vol. 36, no. 1, pp. 131–138, Jan./Feb. 2000.

[8] C. Guzman, A. Cardenas, and K. Agbossou, "Load sharing strategy for autonomous AC microgrids based on FPGA implementation of ADALINE & FLL," *IEEE Trans. Energy Convers.*, pp. 1–10, 2014.

[9] Q.-C. Zhong, "Robust droop controller for accurate proportional load sharing among inverters operated in parallel," *IEEE Trans. Ind. Electron.*, vol. 60, no. 4, pp. 1281–1290, Apr. 2013.

[10] Q.-C. Zhong and Y. Zeng, "Parallel operation of inverters with different types of output impedance," in *Proc. of the IEEE Industrial Electronics Society (IECON)*, Nov. 2013, pp. 1398–1403.

[11] ——, "Can the output impedance of an inverter be designed capacitive?" in *Proc. of the 37th Annual IEEE Conference of Industrial Electronics (IECON)*, Nov. 2011, pp. 1220–1225.

[12] ——, "Control of inverters via a virtual capacitor to achieve capacitive output impedance," *IEEE Trans. Power Electron.*, vol. 29, no. 10, pp. 5568–5578, Oct 2014.

[13] K. D. Brabandere, B. Bolsens, J. V. den Keybus, A. Woyte, J. Driesen, and R. Belmans, "A voltage and frequency droop control method for parallel inverters," *IEEE Trans. Power Electron.*, vol. 22, no. 4, pp. 1107–1115, Jul. 2007.

[14] W. Yao, M. Chen, J. Matas, J. Guerrero, and Z.-M. Qian, "Design and analysis of the droop control method for parallel inverters considering the impact of the complex impedance on the power sharing," *IEEE Trans. Ind. Electron.*, vol. 58, no. 2, pp. 576–588, Feb. 2011.

[15] H. Bevrani and S. Shokoohi, "An intelligent droop control for simultaneous voltage and frequency regulation in islanded microgrids," *IEEE Trans. Smart Grid*, vol. 4, no. 3, pp. 1505–1513, 2013.

[16] H. Khan, S. Dasouki, V. Sreeram, H. Iu, and Y. Mishra, "Universal active and reactive power control of electronically interfaced distributed generation sources in virtual power plants operating in gridconnected and islanding modes," *IET Generation, Transmission & Distribution,*, vol. 7, no. 8, pp. 885–897, Aug. 2013.

[17] X. Sun, Y. Tian, and Z. Chen, "Adaptive decoupled power control method for inverter connected DG," *IET Renewable Power Generation*, vol. 8, no. 2, pp. 171–182, Mar. 2014.

[18] M. Karimi-Ghartemani, "Universal integrated synchronization and control for single-phase dc/ac converters," *IEEE Trans. Power Electron.*, vol. 30, no. 3, pp. 1544–1557, Mar. 2015.

[19] J. He and Y. W. Li, "Analysis, design, and implementation of virtual impedance for power electronics interfaced distributed generation," *IEEE Trans. Ind. Appl.*, vol. 47, no. 6, pp. 2525–2538, 2011. [Online]. Available: http://ieeexplore.ieee.org/stamp/stamp.jsp?arnumber=6022775

[20] Y. Li and Y. W. Li, "Power management of inverter interfaced autonomous microgrid based on virtual frequency-voltage frame," *IEEE Trans. Smart Grid*, vol. 2, no. 1, pp. 30–40, 2011.

[21] Q.-C. Zhong and D. Boroyevich, "A droop controller is intrinsically a phase-locked loop," in *Proc. of the 39th Annual Conference of the IEEE Industrial Electronics Society, IECON 2013*, Vienna, Austria, Nov. 2013, pp. 5916–5921.

[22] D. Poole, *Linear algebra: A modern introduction*, 3rd ed., 2011.

[23] "The grid code," National Grid Electricity Transmission PLC, Tech. Rep., Dec. 2010.

Qing-Chang Zhong (M'04-SM'04) received the Ph.D. degree in control theory and power engineering (awarded the Best Doctoral Thesis Prize) from Imperial College London, London, U.K., in 2004 and the Ph.D. degree in control theory and engineering from Shanghai Jiao Tong University, Shanghai, China, in 2000.

He holds the Max McGraw Endowed Chair Professor in Energy and Power Engineering at the Dept. of Electrical and Computer Engineering, Illinois Institute of Technology, Chicago, USA, and the Research Professor in Control of Power Systems at the Department of Automatic Control and Systems Engineering, The University of Sheffield, UK. He is a Distinguished Lecturer of both the IEEE Power Electronics Society and the IEEE Control Systems Society. He (co-)authored three research monographs: *Control of Power Inverters in Renewable Energy and Smart Grid Integration* (Wiley-IEEE Press, 2013), *Robust Control of Time-Delay Systems* (Springer-Verlag, 2006), *Control of Integral Processes with Dead Time* (Springer-Verlag, 2010), and a fourth, *Power Electronics-enabled Autonomous Power Systems: Next Generation Smart Grids*, is scheduled for publication by Wiley-IEEE Press in 2016. He proposed the architecture for the next-generation smart grids, which adopts the synchronization mechanism of synchronous machines to unify the interface and interaction of power system players with the grid and achieve autonomous operation of power systems. His research focuses on power electronics, advanced control theory and the integration of both, together with applications in renewable energy, smart grid integration, electric drives and electric vehicles, aircraft power systems, high-speed trains etc.

He is a Fellow of the Institution of Engineering and Technology (IET), a Senior Member of IEEE, the Vice-Chair of IFAC TC of Power and Energy Systems and was a Senior Research Fellow of the Royal Academy of Engineering/Leverhulme Trust, UK (2009–2010) and the UK Representative to the European Control Association (2013-2015). He serves as an Associate Editor for *IEEE Transactions on Automatic Control*, *IEEE Transactions on Power Electronics*, *IEEE Transactions on Industrial Electronics*, *IEEE Transactions on Control Systems Technology*, *IEEE Access*, *IEEE Journal of Emerging and Selected Topics in Power Electronics*, *European Journal of Control* and the Conference Editorial Board of the IEEE Control Systems Society.

Yu Zeng received the B.Eng. degree in automation from Central South University, Changsha, China, in 2009. She is currently working toward the Ph.D. degree from the Department of Automatic Control and Systems Engineering, the University of Sheffield, Sheffield, U.K. Her research interests include control of power electronic systems, microgrids and distributed generation, in particular, the parallel operation of inverters.